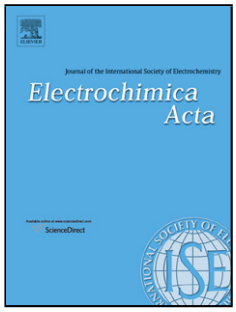

Title: Carbonate anion controlled growth of $LiCoPO_4$/C nanorods and its improved electrochemical behavior

Authors: Ganguli babu, Kalaiselvi Nallathamby, Danielle Meyrick, Manickam Minakshi

PII: S0013-4686(12)01606-4
DOI: doi:10.1016/j.electacta.2012.09.115
Reference: EA 19352

To appear in: *Electrochimica Acta*

Received date: 16-6-2012
Revised date: 27-9-2012
Accepted date: 30-9-2012

Please cite this article as: G. babu, K. Nallathamby, D. Meyrick, M. Minakshi, Carbonate anion controlled growth of $LiCoPO_4$/C nanorods and its improved electrochemical behavior, *Electrochimica Acta* (2010), doi:10.1016/j.electacta.2012.09.115

Carbonate anion controlled growth of $LiCoPO_4$/C nanorods and its improved electrochemical behavior

Ganguli babu[1], Kalaiselvi Nallathamby[1]*, Danielle Meyrick[2], Manickam Minakshi[2]

[1]ECPS Division, Central Electrochemical Research Institute, Karaikudi 630 006, India

[2]School of Chemical and Mathematical Sciences, Murdoch University, Murdoch, WA 6150, Australia

kalaiselvicecri@gmail.com

Tel.: +91-4565-241427

Highlights

Carbonate anion controlled growth of $LiCoPO_4$ nanorods has been prepared.

Mixture of $H_2CO_3 + (NH_4)_2CO_3$ increases the CO_3^{2-} concentration and acts as an effective growth inhibitor.

Heating the carbonate rich precursor in an inert atmosphere produces a Co_2P phase that is conductive.

Addition of super P carbon resulted in an amorphous carbon coating on $LiCoPO_4$ particles.

$LiCoPO_4$/C nanorods with a co-existence of Co_2P exhibit excellent discharge capacity with retention on multiple cycling.

Abstract

$LiCoPO_4$/C nanocomposite with growth controlled by carbonate anions was synthesized via a unique solid-state fusion method. Carbonate anions in the form of H_2CO_3 or a mixture of $H_2CO_3 + (NH_4)_2CO_3$ have been used as a growth inhibiting modifier to produce morphology controlled lithium cobalt phosphate. The presence of cobalt phosphide (Co_2P) as a second phase improved the conductivity and electrochemical properties of the parent $LiCoPO_4$. The formation of Co_2P is found to be achievable only in

an inert atmosphere. Super P® carbon (10 wt. %) provided an adherent carbon coating on pristine $LiCoPO_4$ resulting in the $LiCoPO_4$/C composite cathode. This electrode exhibited enhanced electrochemical properties: capacity of 123 mAh g^{-1} with excellent capacity retention of 89 % after 30 cycles, and reasonable rate capability of up to 5 C rate. The synergistic effect of carbonate anions and formation of Co_2P under inert atmosphere has influenced the electrochemical behavior of $LiCoPO_4$/C cathode through controlling the morphology and increasing the conductivity.

Keywords: carbonate anion; Co_2P; $LiCoPO_4$/C; nanorods; lithium batteries

1. Introduction

Rechargeable lithium batteries are dominating the field of energy devices due to their high specific energy (energy per unit weight) and energy density (energy per unit volume). Associated with the various oxides that have been considered as lithium intercalating cathode materials are major concerns relating to cost, safety and environmental consequences when these cathodes are applied in large-scale lithium-ion batteries. The breakthrough of olivine phosphates with the general formula $LiMPO_4$ [1-5], provides a new class of cathode materials for lithium-ion batteries offering several appealing attributes, including high discharge rate with excellent capacity retention and low cost. Among the available olivine phosphates, low cost lithium iron phosphate ($LiFePO_4$) has attracted particular interest due to its non-toxic and environmentally benign nature and it has been commercialized as a cathode material. However, despite its commercialization, it is inferior to $LiCoPO_4$ and $LiNiPO_4$ cathodes in terms of energy density and other problems [3]. The penetration of $LiMnPO_4$ into the portable electronics market, on the other hand, is hampered by sluggish lithium diffusion kinetics coupled with its extremely low electronic conductivity ($<10^{-10}$ Scm^{-1}) [4-5].

$LiCoPO_4$ has a number of advantages, including high redox potential (4.8 V *vs.* Li^+/Li) with the theoretical energy density of ~ 802 Wh Kg^{-1} (1.35 times higher than that of $LiFePO_4$) [6-8]. $LiCoPO_4$ has additional merits such as better electronic conductivity (about five orders of magnitude higher) than $LiMnPO_4$, lesser threat to electrolyte decomposition compared to $LiNiPO_4$ (with a redox potential of 5.1 V) and the lowest volume change (~2 %) during intercalation and de-intercalation processes among the

studied $LiMPO_4$ (M = Fe, Co, Mn, Ni) cathodes [9-12]. Despite these advantages, there are challenges associated with the practical application of $LiCoPO_4$ [9, 10, 13-16] such as poor conductivity and slow lithium transport kinetics. These must be improved if $LiCoPO_4$ is to be a suitable cathode material alternative.

There are several strategies to overcome the challenges associated with the $LiCoPO_4$ cathode, such as reducing the particle size of the $LiCoPO_4$ material, doping with transition metal atoms and coating the surface with carbon. While coating carbon on the pristine $LiFePO_4$ surface is quite straightforward, the same is not true for the $LiCoPO_4$ counterpart [17]; strong contact between the $LiCoPO_4$ particles is not created. Among the few reports of the preparation of $LiCoPO_4$ cathode [7, 9, 10, 13, 15, 18, 19], Wolfenstine *et al.* [13] have observed the simultaneous formation of cobalt phosphide (Co_2P) when $LiCoPO_4$ is produced in the inert heating environment. The highly conducting (~10^{-1} S cm^{-1}) Co_2P phase formation yields better electrochemical performance of the $LiCoPO_4$ cathode [13]. In separate studies [20, 21], the formation of shape controlled nanocrystalline $LiMPO_4$ (Fe, Mn) was reported to influence the electrochemical behavior due to a shortened diffusion path length for lithium ions. These studies [20, 21] have reported the synthesis of one dimensionally grown nanorods by exploiting the inhibiting effect of CO_3^{2-}.

Hence, the primary objective of this work is to synthesize $LiCoPO_4$/C nanocomposite via a unique solid-state fusion (SSF) method and characterize the controlled growth of $LiCoPO_4$/C nanorods containing the electrochemically active Co_2P phase. Li_2CO_3 as a source of lithium and carbonate anion (H_2CO_3 or $(NH_4)_2CO_3$ + H_2CO_3) as a growth modifier have been used as precursors in this synthesis. An inert

(argon) heating atmosphere has been chosen to trap the carbon within the particles and to facilitate the co-existence of the conductive Co_2P phase in the $LiCoPO_4$/C nanorods. Another objective of this study is to individually examine the growth inhibiting carbonate-containing additives to understand the effect of CO_3^{2-} inhibition on $LiCoPO_4$/C nanorod formation. Synergistic effect of synthesis methodology that renders the formation of $LiCoPO_4$ with desirable Co_2P as second phase, effect of growth inhibiting modifiers in forming nanorods and the improving effect of super P® carbon (10 wt. %) on the electrochemical behavior of the $LiCoPO_4$/C cathode are discussed in this work.

2. Experimental

$LiCoPO_4$ has been prepared by three different routes, namely (a) conventional solid state fusion, (b) modified solid state fusion with the addition of carbonic acid (H_2CO_3) as growth inhibiting modifier, and (c) modified solid state fusion mixture of carbonic acid and ammonium bicarbonate (H_2CO_3+$(NH_4)_2CO_3$).

For conventional solid-state fusion route, stoichiometric amounts of lithium carbonate (Li_2CO_3), cobalt carbonate ($CoCO_3$) and ammonium dihydrogen phosphate ($NH_4H_2PO_4$) (Alfa Aesar, 99%) were ball milled for 12 h and the resultant powder collected in a crucible. The powder was initially heated at 300 °C for 8 h to eliminate the gaseous products and the mixture was then calcined at 700 °C for 8 h with intermittent grinding to avoid particle agglomeration. The final product thus obtained was $LiCoPO_4$. The modified solid-state fusion procedure was as above, with additional treatment of growth inhibiting modifiers (either H_2CO_3 alone, or a solution of H_2CO_3 + $(NH_4)_2CO_3$) by covering the solid precursor mixture in the crucible with the inhibitor solution and sonicating the content for 30 minutes to ensure percolation of growth inhibitor solution

through the solid mixture. In other words, 30 ml of carbonic acid has been added to maintain the precursor mix in wet condition even after sonication and the amount of $(NH_4)_2CO_3$ used in the experiments was 1.5 g. Higher CO_3^{2-} concentrations (aided by the addition of H_2CO_3 and H_2CO_3 + $(NH_4)_2CO_3$ mix) confine the growth of crystals in one dimension, leading to porous $LiCoPO_4$ nanorods [21]. The escape of CO_2 gas and the growth inhibited formation of nanorods aided by the addition of H_2CO_3 are documented in our previous report [20].

$LiCoPO_4$ synthesized by different routes (labeled as Samples 'A1', 'B1' and 'C1') was similarly synthesized in an argon atmosphere, with all other conditions unchanged, to produce Samples 'A2', 'B2' and 'C2'. Subsequently, samples 'A2', 'B2' and 'C2' were treated further to obtain $LiCoPO_4$/C composite by the following procedure. The three $LiCoPO_4$ parent compounds (synthesized in argon atmosphere) were ball milled individually with 10 wt. % super P® carbon for approximately 12 h. The product was furnace heated at 500 °C (2 h) in argon atmosphere to obtain respective $LiCoPO_4$/C composites (labeled as Samples 'A3', 'B3' and 'C3'). The electrode preparation from the synthesized $LiCoPO_4$/C powder and coin cell fabrication was according to methods previously reported [20].

The native $LiCoPO_4$ and nanocomposites of $LiCoPO_4$/C thus obtained were systematically physically and electrochemically characterized. X-ray powder diffraction patterns of synthesized compounds were recorded on a PANalytical X'pert PRO X-ray diffractometer using Ni-filtered Cu Kα radiation (λ = 1.5406 Å) in the 2θ range of 10–70° and at a scan rate of 3° per minute. Conductivity measurements were carried out using LCR meter (Hioki-3532) in the temperature range 100 to 400 °C and frequency range 42

to 1 MHz. Surface morphology of synthesized samples were studied on a scanning electron microscope (JSM 6400, JEOL, Japan). Transmission electron microscope (TEM) images were collected using a JEOL 2010F TEM operating at 200 keV. A Raman spectrum was analyzed using a Renishaw InVia Laser Raman Microscope. The oxidation state of elements in $LiCoPO_4$ compound was investigated by X-ray photoelectron spectroscopy (XPS) using an Mg Kα excitation source. Charge-discharge studies were carried out using ARBIN charge-discharge cycle life tester at a constant charge-discharge rate of 0.1 C.

3. Results and discussion

3.1. Structural studies: XRD

The X-ray diffraction (XRD) patterns of the pristine $LiCoPO_4$ powder synthesized via conventional solid state fusion (SSF) (Sample 'A1'), modified solid state fusion with the addition of H_2CO_3 (Sample 'B1') and H_2CO_3 + $(NH_4)_2CO_3$ (Sample 'C1') in an oxidizing (air) environment are shown in Fig. 1. All of the reflections could be indexed on the basis of the ordered olivine structure with an orthorhombic Pnmb space group (ICDD pattern 32-0552). The sharp diffraction peaks illustrate the obtained product is highly crystalline. The absence of second phases such as Co_3O_4 or $Co_2P_2O_7$ in the synthesized $LiCoPO_4$ powder indicates the formation of phase-pure samples [22]. A more detailed analysis of the XRD pattern (in Fig. 1c) reveals the presence of Li_3PO_4 as a minor phase in Sample 'C1'. No detectable reflections corresponding to Co_2P phase are present in all the synthesized samples (Fig. 1a-c), indicating an oxidizing environment does not support its formation, a finding substantiated by Wolfenstein *et al.* [13]. An

identical set of samples have been prepared in the argon atmosphere while keeping the other conditions unchanged to obtain Samples 'A2', 'B2' and 'C2'.

Fig. 2 (a-c) shows the X-ray diffraction (XRD) patterns of the pristine $LiCoPO_4$ powder (Samples A2, B2 and C2). The presence of Co_3O_4 as a second phase together with the major olivine ($LiCoPO_4$) phase is observed in Sample A2 (conventional SSF) (Fig. 2a). The modified SSF method with the addition of H_2CO_3 produced a single phase (Fig. 2b) of olivine structure (ICDD pattern 32-0552). Interestingly, $LiCoPO_4$ compound synthesized with the addition of H_2CO_3 + $(NH_4)_2CO_3$ (Fig. 2c) showed $LiCoPO_4$ peaks along with those for the highly conductive Co_2P phase [23]. An increased concentration of CO_3^{2-} anion (through the addition of $(NH_4)_2CO_3$) has influenced the phase purity of nanocrystalline $LiCoPO_4$ by co-producing Co_2P. Hence, the synergistic effect of CO_3^{2-} ion concentration and the presence of an inert argon atmosphere aided in producing $LiCoPO_4$ as a major phase with the co-existence of conductive Co_2P.

3.2. Conductivity Studies

The ionic conductivity (ac) of the conventional (Sample A1, A2) and modified solid state fusion synthesized $LiCoPO_4$ (Samples B1, B2 and C1, C2) synthesized in air and argon atmospheres has been investigated in the temperature range 30 – 400 °C (Figs 3 and 4). The ionic conduction in the $LiCoPO_4$ cathode is due to movement of ions by hopping mechanism between the allowed sites. Irrespective of the synthesis conditions, for all samples conductivity at low frequencies is frequency-independent (characterized by a plateau in the curve), while at higher frequencies, a dispersion region is observed in the conductivity plot. The former and latter behaviour correspond to the DC and AC conductivity of the bulk $LiCoPO_4$ respectively. Extrapolation of the plateau to the *Y*-axis

gives the DC conductivity [24]; values obtained at 100 and 400 °C are given in Table 1. At a higher temperature (400 °C), a two-fold increase in conductivity has been observed in all the $LiCoPO_4$ samples (Figs. 3-4) relative to that the values observed at lower temperature. The highest conductivity was exhibited by $LiCoPO_4$ obtained in the presence of H_2CO_3 + $(NH_4)_2CO_3$ and heat treated under an argon atmosphere. This sample, which according to XRD analysis contained highly conducting Co_2P, showed an increase in conductivity from the order of 10^{-8} at 100 °C to 10^{-6} S cm^{-1} 400 °C.

Based on these results, it is understood that $LiCoPO_4$ sample synthesised in the presence of H_2CO_3+$(NH_4)_2CO_3$ and heat treated under argon atmosphere has properties desirable for lithium intercalation behavior. Hence, samples ('A3', 'B3' and 'C3') are chosen for further studies.

3.3. Microscopy & Spectroscopy Studies: SEM, TEM, Raman and XPS

Fig. 5 shows the scanning electron microscopy (SEM) images of the $LiCoPO_4$/C nanocomposites prepared as described above in an argon atmosphere (Samples 'A3', 'B3' and 'C3'). The presence of agglomerated $LiCoPO_4$ particles with spherical shapes is evidenced from the SEM images (Fig. 5a) for conventionally-synthesized (i.e., no modifier) sample (Sample 'A3'). On the other hand, needle and rod-like morphologies are observed (Fig. 5b-c) for samples synthesized by modified SSF (Samples 'B3' and 'C3'). The morphological transformation, from spherical to rod, implies the crystal growth has been controlled to the one dimension when carbonate anions are present. A higher concentration of carbonate anions (Sample 'C3') led to the rod like morphology (Fig. 5c) The appearance of shiny particles in all images (Fig. 5a-c) corresponds to the

presence of added super P® carbon in $LiCoPO_4$/C composite, which is in agreement with the expected behavior.

Transmission electron microscopy (TEM) images recorded for $LiCoPO_4$/C composites (Samples 'A3', 'B3' and 'C3') synthesized in argon atmosphere are shown in Fig. 6. The presence of nanocrystalline $LiCoPO_4$/C composite with an adherent carbon coating is evident in Fig. 6 (a-c). A change in morphology evidenced from the TEM images substantiates the SEM results. A thick layer of carbon coating seen in the TEM images illustrates the carbon layer encapsulated the $LiCoPO_4$ particles. A continuous carbon coating on the surface of native $LiCoPO_4$ particles suggests the chosen synthetic conditions are optimum to form nanocomposites. The presence of carbon network interconnects the individual particles of $LiCoPO_4$, leading to carbon wiring that enhances the electrochemical behavior of the synthesized $LiCoPO_4$/C composite cathodes.

It is well known that the electrochemical performance of any composite electrode depends upon the type and nature of carbon involved and hence Raman spectroscopy has been used to investigate the nature of super P® carbon used in this study. In this regard, $LiCoPO_4$/C (Sample 'B3') powder, obtained from the addition of H_2CO_3 and heat treated in argon atmosphere (which has been demonstrated to form a single phase compound, as indicated by XRD, Fig. 2b) has been chosen as a typical compound for Raman spectroscopy studies. The recorded spectrum **(**Fig. 7) shows two characteristic broad bands around 1598 (G-band) and 1332 cm^{-1} (D-band) characteristic of ordered graphitic and amorphous carbon respectively [25-26]. The ratio of the calculated peak intensities (I_D/I_G) demonstrates that amorphous carbon is dominant, which could favor lithium intercalation.

The sample 'B3' was further characterized by X-ray photoelectron spectroscopy (XPS) to confirm the oxidation state of the individual elements present in the compound (Fig. 8). Herein, peaks corresponding to those of Li (1s), Co ($2p_{3/2}$), P ($2p_{3/2}$) and O (1s) in the $LiCoPO_4$ cathode observed at the respective binding energy values correspond well with the reported values [27-28]. Particularly, the Li (1s) spectrum consists of a peak at 55.8 eV that confirms the oxidation state of Li as +1 and the best fit for the Co $2p_{3/2}$ spectrum gives a binding energy value of 780.7 eV, which is consistent with the value reported to those for Co^{2+} ions by Tan et al. [27]. The XPS spectra for the P (2p) peak located at 134.1 eV is assigned to the P^{5+} related compounds [28]. The O (1s) XPS spectrum has a well defined peak at 531.0 eV evidencing the presence of -2 oxidation state of O element in $LiCoPO_4$.

3.4. Electrochemical Studies: Charge-discharge and Rate capability tests

Fig. 9a shows the typical galvanostatic charge-discharge profile of a lithium coin cell consisting of $LiCoPO_4$/C nanocomposite cathode coupled with a metallic lithium anode. The cut-off voltages used for discharge and charge cycle are 3.0 and 5.1 V respectively. The cell was charged and discharged at a constant rate of 0.1 C. The charge-discharge characteristics for all the samples are similar in shape, exhibiting a plateau each at about 4.8 and 4.7 V respectively, corresponding to $Co^{3+/2+}$ redox couple. The observed small difference of 0.1 V between the charge and discharge plateau illustrates that the electrochemical polarization is small. This could be attributed to the formation of one dimensional and morphological growth controlled $LiCoPO_4$ nanorods, which facilitate the faster diffusion of lithium ions.

Although the electrochemical characteristics appear to be similar, the discharge capacities are found to be different for the electrode material prepared by the chosen synthetic routes with a small potential drop. The higher charge and discharge capacity of 162 and 123 mAh g^{-1} were observed for the sample containing the highest concentration of carbonate anions (Sample 'C3'). The charge and discharge capacities observed for samples 'A3' are found to be only 120 and 64 while those for 'B3' are 140 and 106 mAh g^{-1} respectively. Thus, the presence of H_2CO_3+$(NH_4)_2CO_3$ enhances the one dimensional growth, and the co-existence of Co_2P phase that influenced the electrochemical behavior of sample 'C3'.

Figure 9b shows the initial discharge capacity of the $LiCoPO_4$/C (Sample 'C3') cathode is 123 $mAhg^{-1}$ and the available capacity after 30 cycles is 109 $mAhg^{-1}$, corresponding to excellent capacity retention of 89 %. On the other hand, other $LiCoPO_4$/C (Samples 'A3' and 'B3') cathodes exhibited not only a lower initial capacity (64 and 106 $mAhg^{-1}$) but also exhibited capacity fade to the extent of 20 and 13 % respectively after the completion of 30 cycles. The enhanced performance of the Sample 'C3' cathode is attributed to the synergistic effects of (a) controlled morphology derived from the modified solid state fusion method with the mixture of growth inhibitors H_2CO_3 + $(NH_4)_2CO_3$, (b) co-existence of conductive Co_2P phase resulting from argon atmosphere and (c) the carbon wiring resulted from externally added super P® carbon.

Rate capability of $LiCoPO_4$/C (Samples 'A3', 'B3' and 'C3') cathodes has been investigated under the influence of C/10, C/5, 1C, 2C and 5C discharge rates and the results are given in Fig. 9c. It is evident that appreciable discharge capacity values of 122, 114, 102, 93 and 81 $mAhg^{-1}$ have been exhibited by $LiCoPO_4$/C (Sample 'C3') cathode

at C/10, C/5, 1C, 2C and 5C rates respectively against the lower capacity values of 106, 95, 86, 79 and 66 $mAhg^{-1}$ corresponding to $LiCoPO_4$/C (Sample 'B3') cathode and those of 64, 52, 42, 31 and 21 $mAhg^{-1}$ exhibited by $LiCoPO_4$/C (Sample 'A3') cathode. It seems that the influence of growth inhibitor $H_2CO_3 + (NH_4)_2CO_3$ (Sample 'C3') in the $LiCoPO_4$/C cathode is to improve the electrochemical behavior. The cathode produced by this method is found to be suitable for high rate lithium battery applications.

4. Conclusions

A simple and an easy-to-adopt modified solid state fusion method has been employed to achieve morphologically controlled growth of $LiCoPO_4$/C nanorods using $H_2CO_3 + (NH_4)_2CO_3$ growth modifiers and heat treatment in an inert (argon) atmosphere. The role of CO_3^{2-} ion in controlling the growth of particles to form rod-like morphology is analysed from microscopic images. The presence of an argon atmosphere during furnace heating, especially with an increased concentation of CO_3^{2-} ion, aids the formation of desirable Co_2P phase. Addition of super P® carbon (10 wt. %) to the $LiCoPO_4$ cathode resulted in an amorphous carbon coating with an improved electronic conductivity and electrochemical performance. A discharge capacity of 123 $mAhg^{-1}$ with excellent capacity retention and good rate capability of up to 5 C rate is attributed to the synergistic effect of controlled growth, co-existence of conductive cobalt phosphide (Co_2P) phase and the presence of amorphous carbon coating on $LiCoPO_4$ particles.

Acknowledgement

Gangulibabu is thankful to Council of Scientific Research (CSIR), India for the financial support through Senior Research Fellowship (SRF). Dr. N. Kalaiselvi is thankful to CSIR for financial support through CSIR Empower Scheme.

References

1. Y. G. Wang, Y. R. Wang, E. Hosono, K. X. Wang, H. Zhou, Angew. Chem. Int. Ed. **47** (2008) 7461.
2. B. Kang, G. Ceder, Nature **458** (2009) 190.
3. Y. Huang, H. Ren, S. Yin, Y. Wang, Z. Peng, Y. Zhou, J. Power Sources **195** (2010) 610.
4. C. Delacourt, L. Laffont, R. Bouchet, C. Wurm, J. B. Leriche, M. Morcette, J. M. Tarascon, C. Masquelier, J. Electrochem. Soc. **152** (2005) A913.
5. K. Rassouli, K. Benkhouja, J. R. Ramos-Barrado, C. Julien, Mater. Sci. Eng. B **98** (2003) 185.
6. F. Wang, J. Yang, Y. NuLi, J. Wang, J. Power Sources **196** (2011) 4806.
7. T. N. L. Doan, I. Taniguchi, J. Power Sources **196** (2011) 5679.
8. F. Wang, J. Yang, Y. Nuli, J. Wang, J. Power Sources **195** (2010) 6884.
9. N. N. Bramnik, K. G. Bramnik, C. Baehtz, H. Ehrenberg, J. Power Sources **145** (2005) 74.
10. N. N. Bramnik, K. Nikolowski, C. Baehtz, K. G. Bramnik, H. Ehrenberg, Chem. Mater. **19** (2007) 908.

11. A. Andersson, B. Kalska, L. Haggstrom, J. Thomas, Solid State Ionics **130** (2000) 41.

12. C. Delacourt, P. Poizot, M. Morcrette, J. -M. Tarascon, C. Masquelier, Chem. Mater. 16 (2004) 93.

13. J. Wolfenstine, J. Read, J. L. Allen, J. Power Sources **163** (2007) 1070.

14. N. N. Bramnik, K. Nikolowski, D. M. Trots, H. Ehrenberg, Electrochem. Solid State Lett., **11** (2008) A89.

15. D.-W. Han, Y. -M. Kang, R. -Z. Yin, M. -S. Song, H. -S. Kwon, Electrochem. Commun. **11** (2009) 137.

16. H. H. Li, J. Jin, J. P. Wei, Z. Zhou, J. Yan, Electrochem. Commun. **11** (2009) 95.

17. J. S. Yang, J. J. Xu, J. Electrochem. Soc. **153** (2006) A716.

18. J. Yang, J. J. Xu, J. Electrochem. Soc. **153** (2006) A716.

19. T. N. L. Doan, I. Taniguchi, Powder Technol., **217** (2012) 574.

20. Gangulibabu, N. Kalaiselvi, D. Bhuvaneswari, C. H. Doh, Int. J. Electrochem. Sci., **5** (2010) 1597.

21. H. Fang, L. Li, Y. Yang, G. Yan, G. Li, Chem. Comm., 2008, 1118.

22. M. S. Bhuvaneswari, L. Dimesso, W. Jaegermann, J. Sol-Gel Sci. Technol. **56** (2010) 320.

23. J. Wolfenstine, J. Power Sources **158** (2006) 1431.

24. M. Vijayakumar and S. Selvasekarapandian, Mater. Res. Bull., **38** (2003) 1735.

25. E. Markevich, R. Sharabi, O. Haik et al, J. Power Sources **196** (2011) 6433.

26. R. Sharabi, E. Markevich, V. Borgel et al, Electrochem. Commun. **13** (2011) 800.

27. L. Tan, Z. Luo, H. Liu, Y. Yu, J. Alloys and Compd. **502** (2010) 407.

28. L. Dimesso, S. Jacke, C. Spanheimer, W. Jaegermann, J. Solid State Electrochem. **16** (2012) 911.

Table 1 Conductivity values of $LiCoPO_4$ compound synthesized using (a) conventional and (b) modified solid state fusion (SSF) method with the addition of growth inhibiting modifier carbonic acid (H_2CO_3) and (c) with a mixture of carbonic acid and ammonium carbonate (H_2CO_3+$(NH_4)_2CO_3$) in air and argon atmospheres.

Methodology / Sample	Atm.	Conductivity / ohm^{-1} cm^{-1} at 100 °C	400 °C
(a) Conventional SSF /A1	Air	**3.9×10^{-9}**	**2.0×10^{-7}**
(b) Modified SSF with the addition of carbonic acid (H_2CO_3) / B1		**9.1×10^{-9}**	**5.1×10^{-7}**
(c) Modified SSF with the addition of carbonic acid (H_2CO_3) and ammonium carbonate (H_2CO_3+$(NH_4)_2CO_3$) / C1		**8.2×10^{-9}**	**3.4×10^{-7}**
(a) Conventional SSF / A2	Argon	**2.6×10^{-9}**	**6.8×10^{-7}**
(b) Modified SSF with the addition of carbonic acid (H_2CO_3) / B2		**4.5×10^{-9}**	**1.9×10^{-7}**
(c) Modified SSF with the addition of carbonic acid (H_2CO_3) and ammonium carbonate (H_2CO_3+$(NH_4)_2CO_3$) / C2		**4.9×10^{-8}**	**6.3×10^{-6}**

Figure Caption

Fig. 1 XRD patterns of the $LiCoPO_4$ synthesized in air using (a) conventional and (b) modified solid state fusion method with the addition of growth inhibiting modifier carbonic acid (H_2CO_3) and (c) with a mixture of carbonic acid and ammonium carbonate (H_2CO_3+$(NH_4)_2CO_3$).

Fig. 2 XRD patterns of the $LiCoPO_4$ synthesized in argon using (a) conventional and (b) modified solid state fusion method with the addition of growth inhibiting modifier carbonic acid (H_2CO_3) and (c) with a mixture of carbonic acid and ammonium carbonate (H_2CO_3+$(NH_4)_2CO_3$).

Fig. 3 Conductance plot of $LiCoPO_4$ synthesized in air using (a) conventional and (b) modified solid state fusion method with the addition of growth inhibiting modifier carbonic acid (H_2CO_3) and (c) with a mixture of carbonic acid and ammonium carbonate (H_2CO_3+$(NH_4)_2CO_3$).

Fig. 4 Conductance plot of $LiCoPO_4$ synthesized under argon atmosphere using (a) conventional and (b) modified solid state fusion method with the addition of growth inhibiting modifier carbonic acid (H_2CO_3) and (c) with a mixture of carbonic acid and ammonium carbonate (H_2CO_3+$(NH_4)_2CO_3$).

Fig. 5 SEM images of $LiCoPO_4$/C synthesized under argon atmosphere using (a) conventional (b) modified solid state fusion method with the addition of growth inhibiting H_2CO_3 modifier and (c) with a mixture of H_2CO_3+$(NH_4)_2CO_3$.

Fig. 6 TEM images of $LiCoPO_4$/C synthesized under argon atmosphere using (a) conventional (b) modified solid state fusion method with the addition of growth inhibiting H_2CO_3 modifier and (c) with a mixture of H_2CO_3+$(NH_4)_2CO_3$.

Fig. 7 Raman spectroscopy of $LiCoPO_4$/C (sample 'B3') composite with added super P carbon as a carbon source.

Fig. 8 XPS spectra of Co ($2p_{3/2}$), P ($2p_{3/2}$) and O (1s) in $LiCoPO_4$/C (sample 'B3') compound.

Fig. 9 Electrochemical behavior of $LiCoPO_4$/C cathodes (samples 'A3', 'B3' and 'C3') vs. Li/Li^+ (a) voltage *vs.* specific capacity (b) capacity *vs.* cycling and (c) rate capability behavior

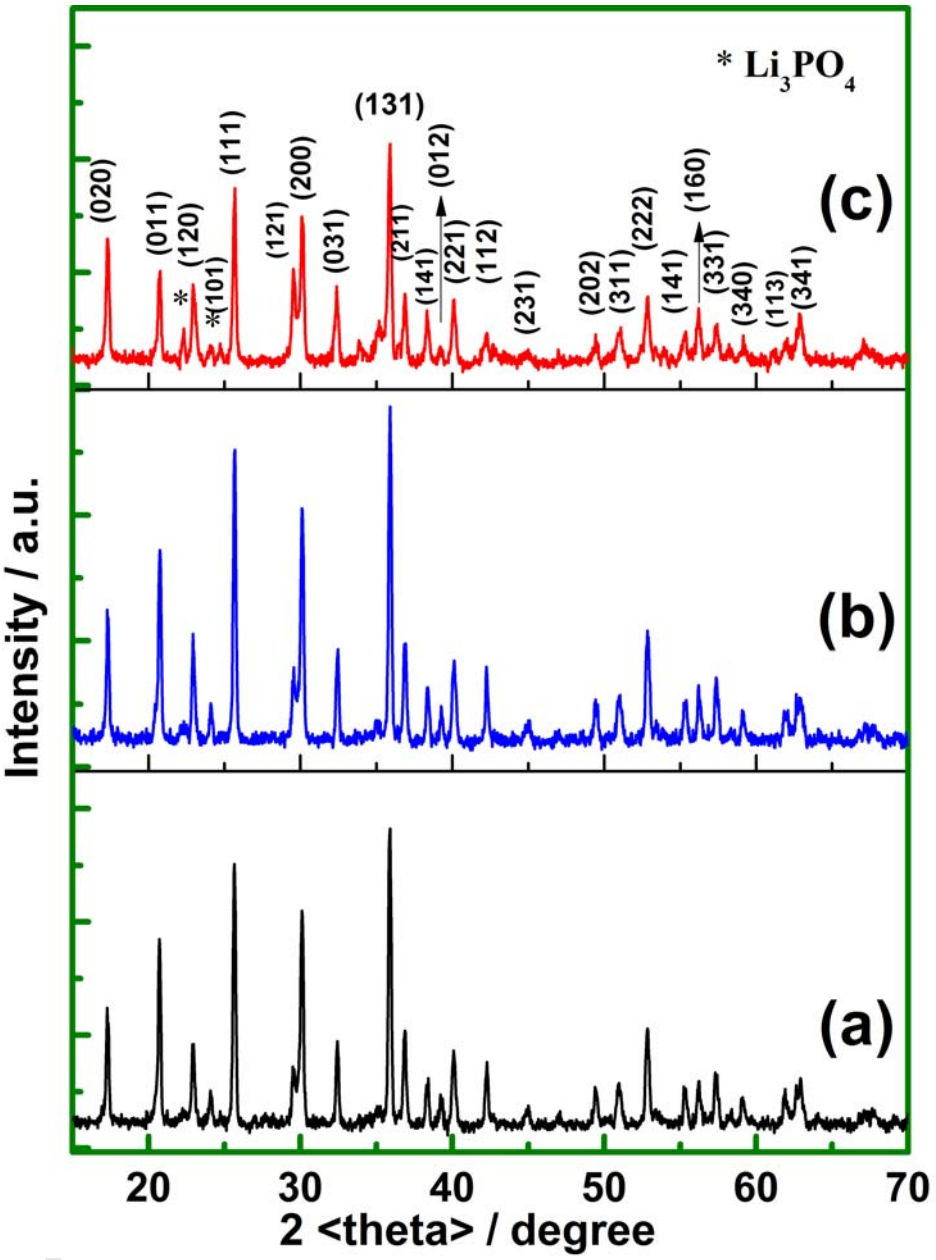

Fig. 1

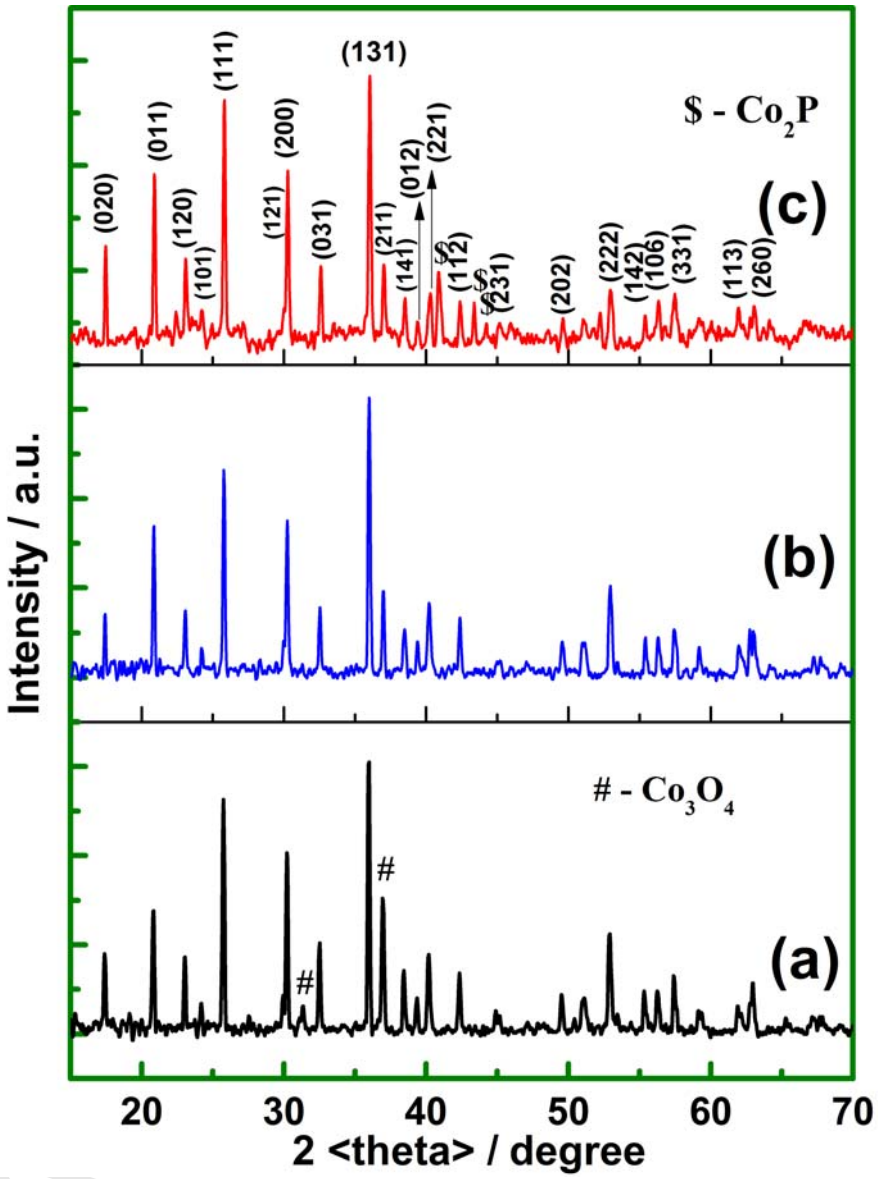

Fig. 2

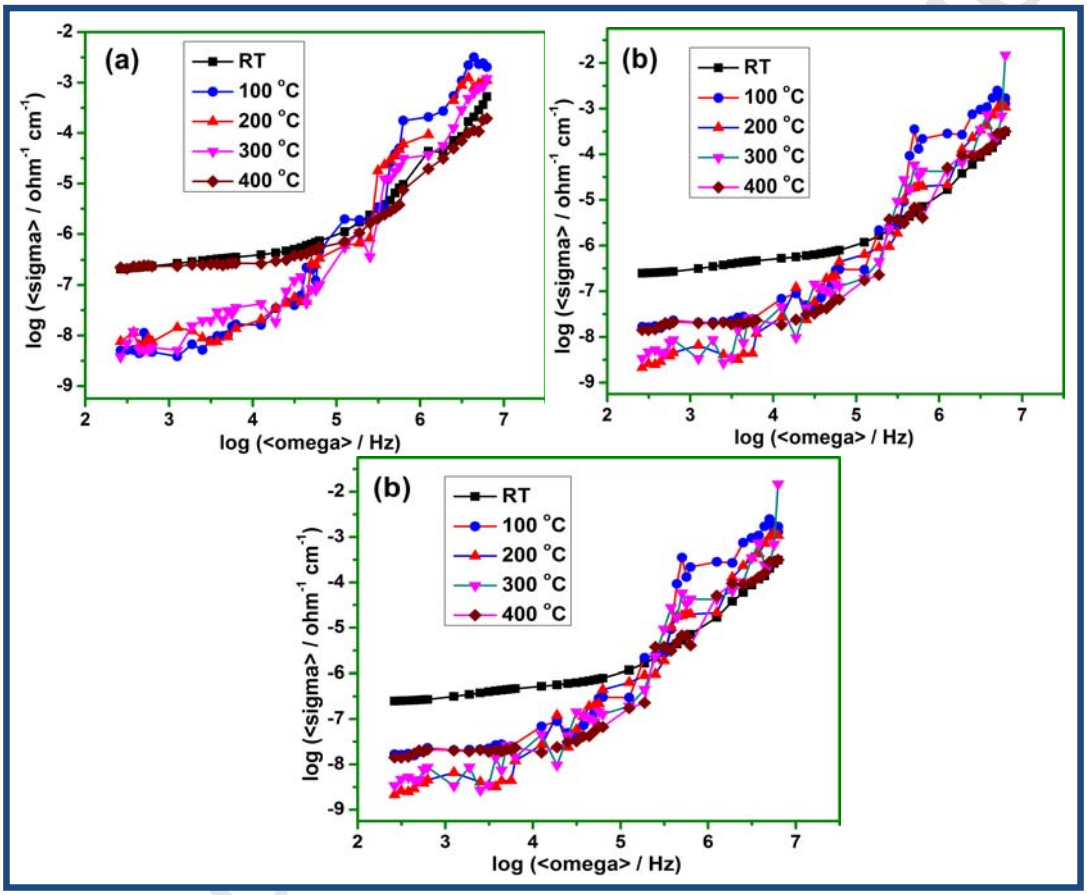

Fig. 3

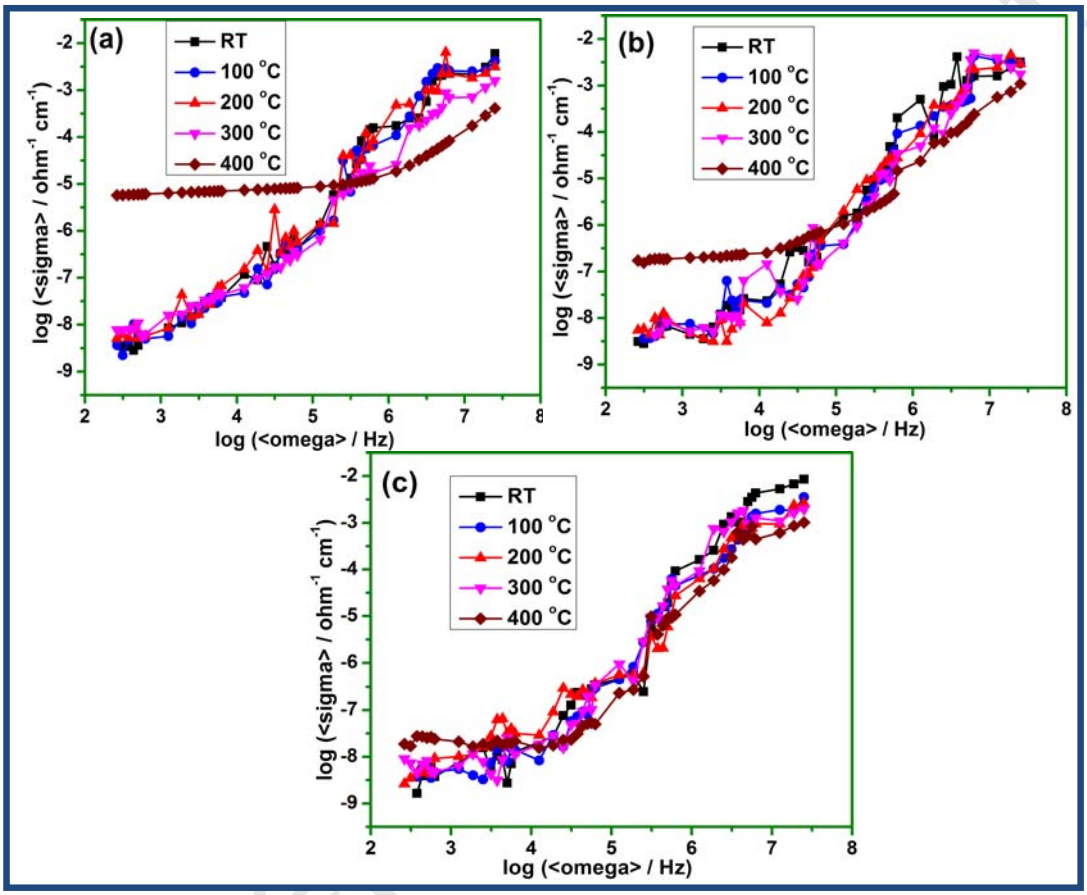

Fig. 4

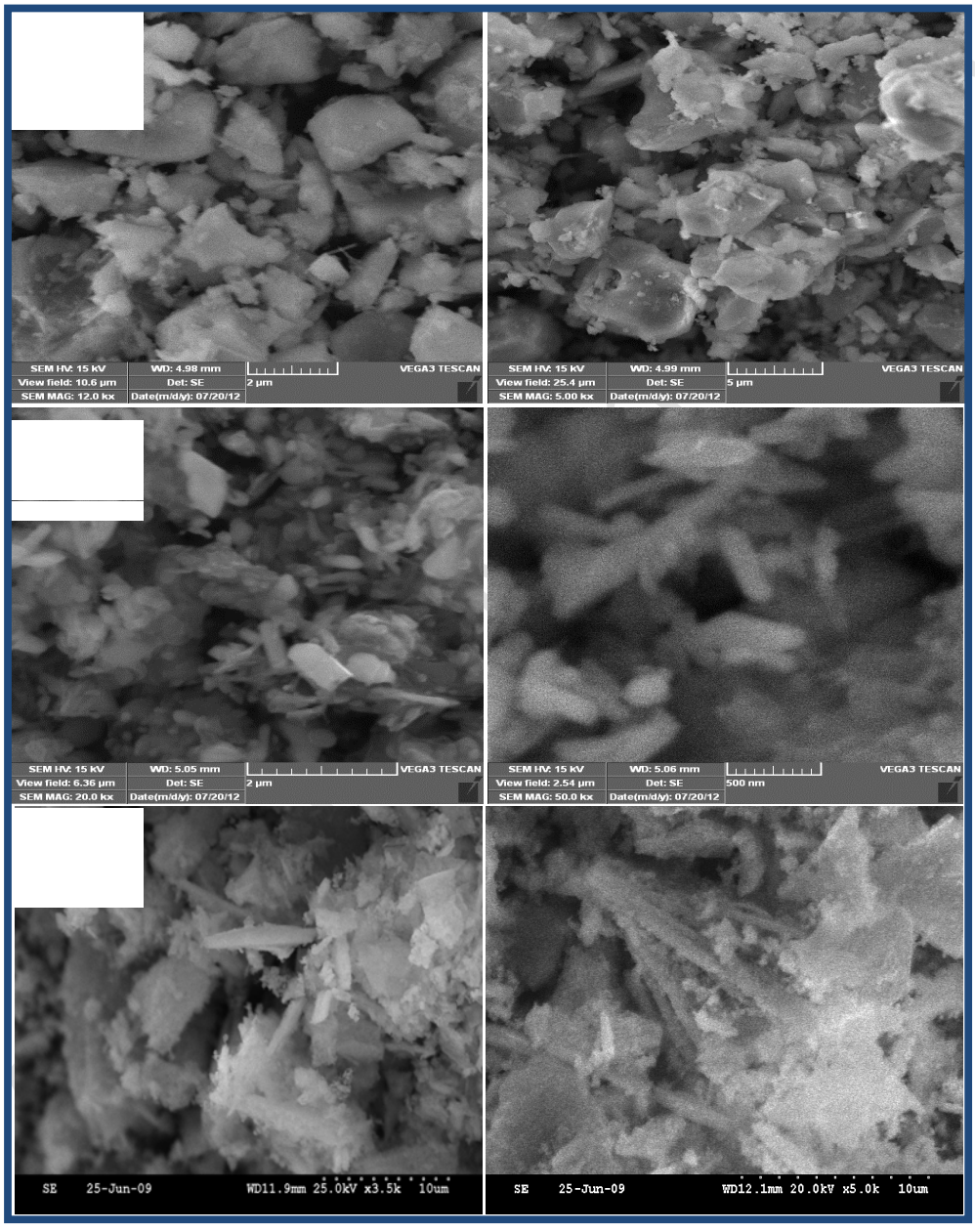

Fig. 5

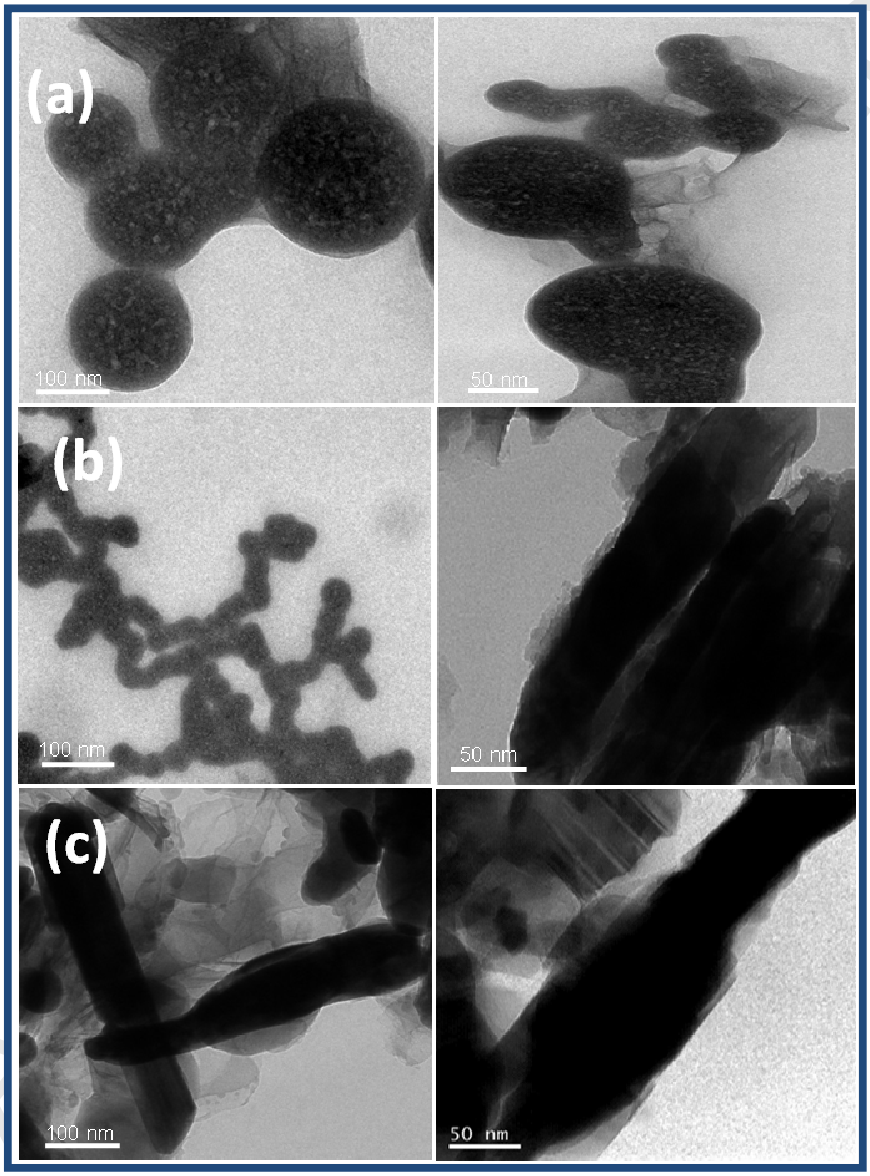

Fig. 6

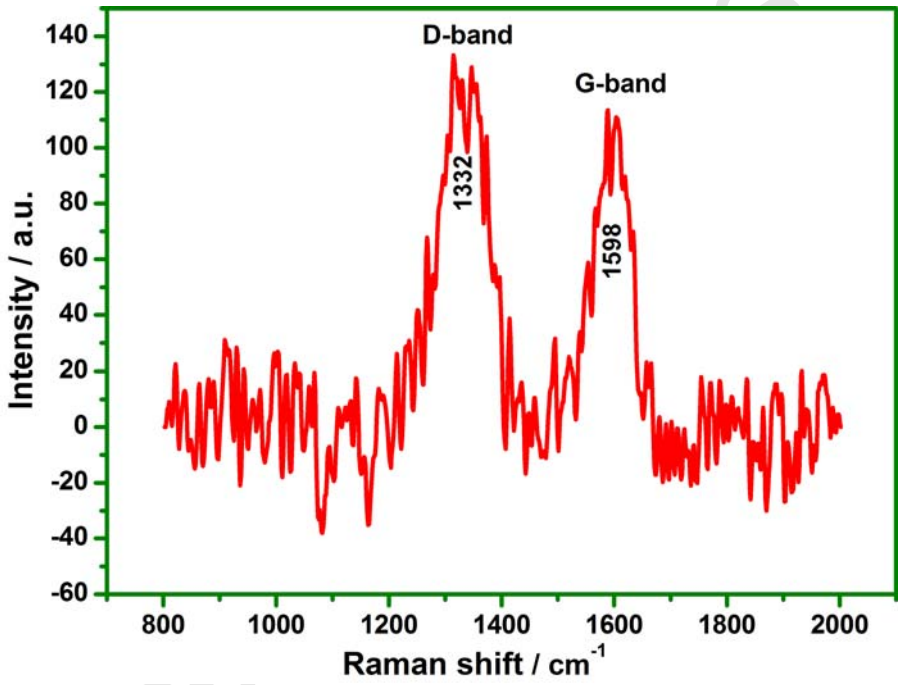

Fig. 7

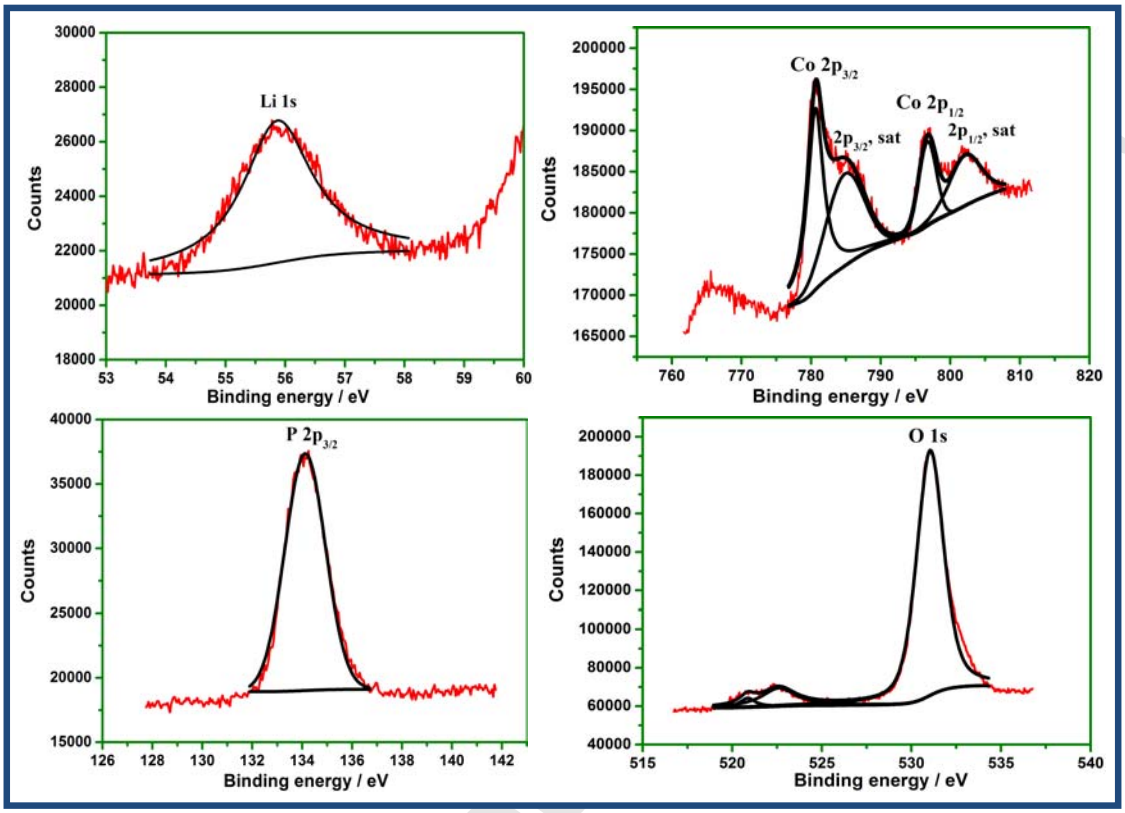

Fig. 8

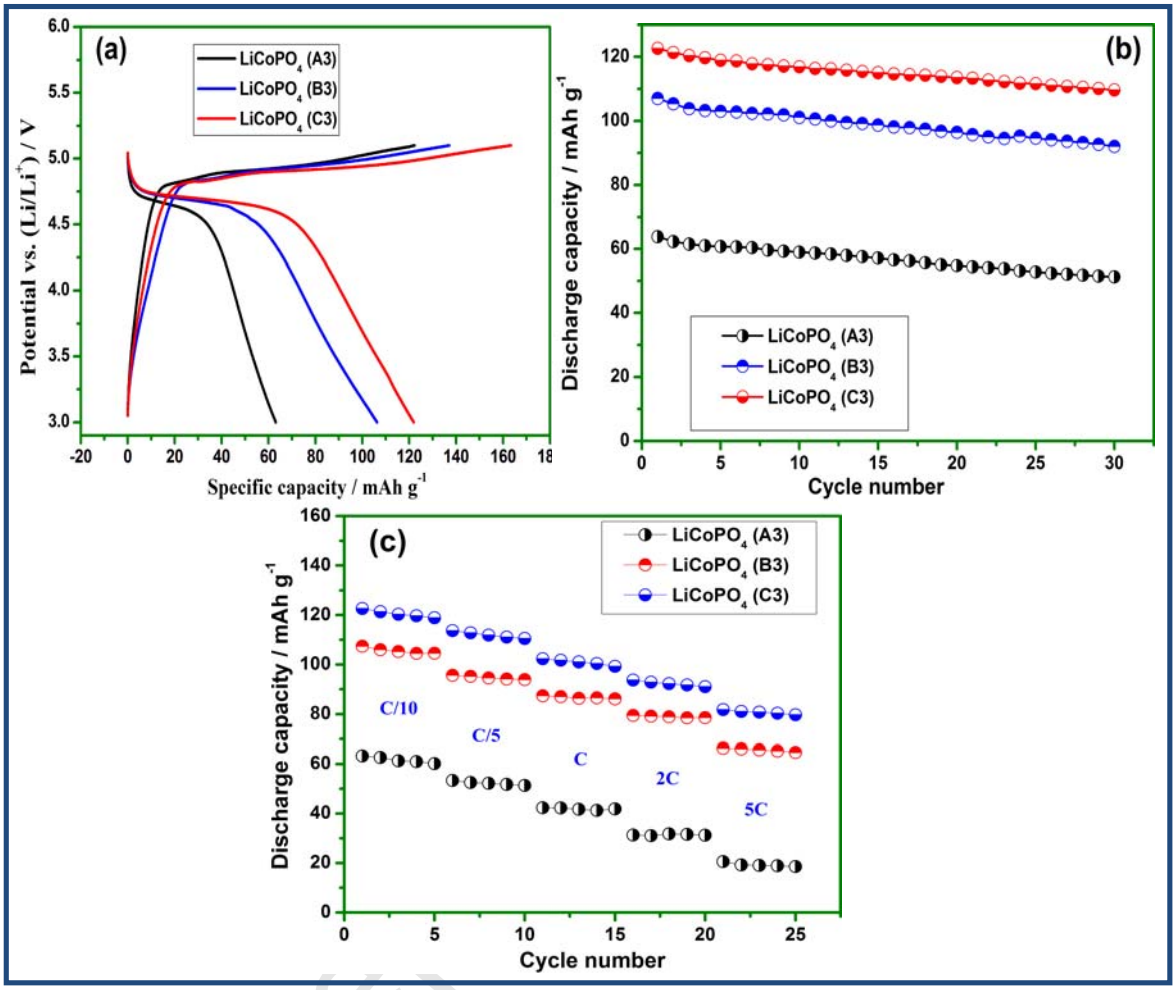

Fig. 9